8 Supplementary material for LHCb-PAPER-2017-007

This appendix contains supplementary material that will be posted on the public cds record but will not appear in the paper.

8.1 Significance of the fraction $\frac{N_{\eta_c(2S)}}{N_{\eta_c(1S)}}$

Figure 12 shows the increase in χ^2 with respect to the best fit value as a function of the $N_{\eta_c(2S)}/N_{\eta_c(1S)}$ yield ratio, taking into account only the statistical uncertainties. The ratio is different from zero with a significance of 3.7 standard deviations.

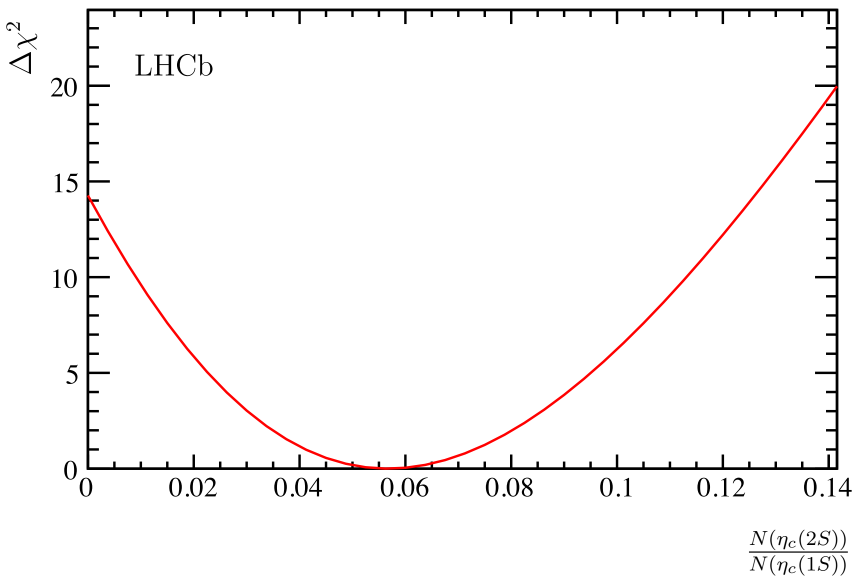

Figure 12: Change in χ^2 with respect to the best fit value as a function of the $\frac{\eta_c(2S)}{\eta_c(1S)}$ yield ratio.

8.2 Comparison between different results of $b \to \chi_c X$

Figure 13 shows a summary of the branching fraction measurements for inclusive decays of light B-mesons, $\mathcal{B}(B \to \chi_c X)$, and of mixtures of all b hadrons, $\mathcal{B}(b \to \chi_c X)$. Also indicated are the PDG averages and averages including the results from this paper. The LHCb result for b-hadron decays to χ_{c0} is the only available result and is not shown in the figure.

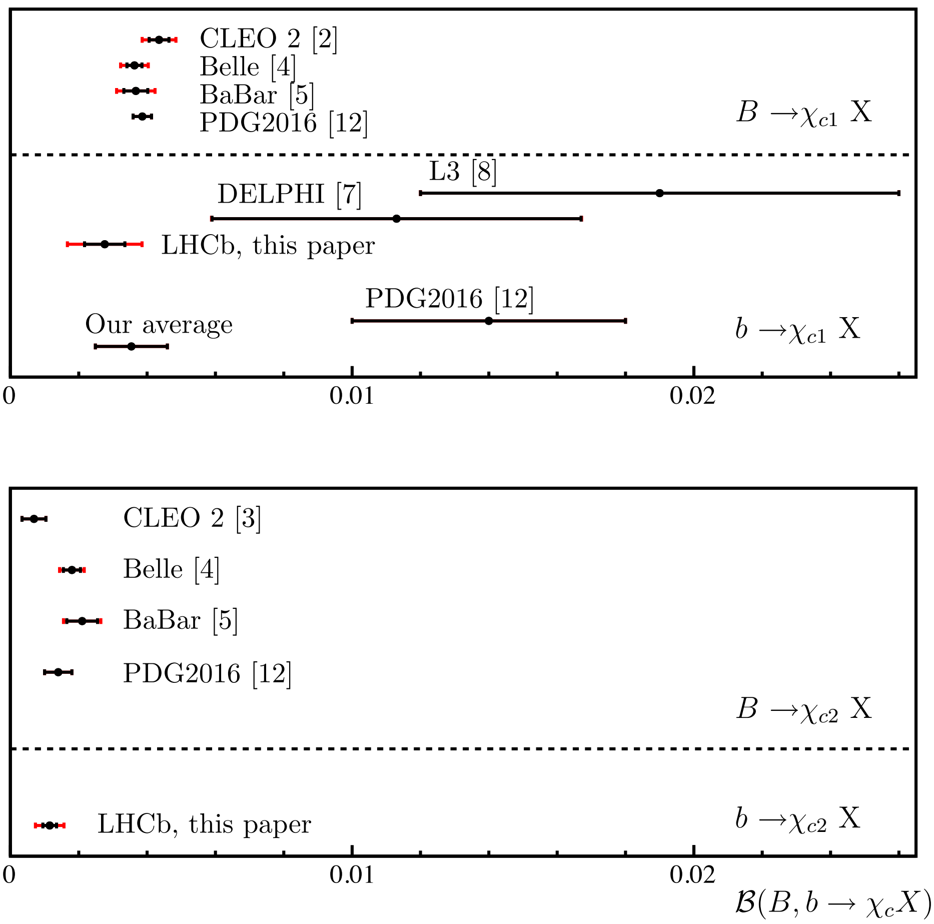

Figure 13: Summary of the branching fraction measurements for inclusive decays of light B mesons, $\mathcal{B}(B \to \chi_c X)$, and of all b hadrons, $\mathcal{B}(b \to \chi_c X)$, shown in each plot above and below the dashed line, respectively. The branching fractions for the decays to χ_{c1} and χ_{c2} are shown in the top and bottom plots, respectively. The world averages noted "PDG2016" do not include the LHCb results.

8.3 Decomposition of the systematic uncertainties for charmonium mass measurements

The list of the systematic uncertainties for the charmonium mass measurements is shown in Table 7.

Table 7: Systematic uncertainties in the measurement of charmonium masses and natural widths in MeV.

Systematic uncertainty	$M_{\eta_c(1S)}$	$M_{\chi_{c0}}$	$M_{\chi_{c1}}$	$M_{\chi_{c2}}$	$M_{\eta_c(2S)}$	$\Gamma_{\eta_c(1S)}$
Including other states	0.01	0.02	< 0.01	0.08	0.01	0.55
Description of detector resolution	0.02	0.02	0.04	0.03	0.13	0.64
Description of signal resonances	< 0.01	< 0.01	< 0.01	< 0.01	0.19	0.14
Background model	0.04	0.05	0.05	0.10	0.21	1.58
2D fit functions	0.11	0.05	0.03	0.01	0.02	0.89
Momentum scale calibration	0.43	0.62	0.66	0.66	0.69	–
Total	0.45	0.62	0.66	0.66	0.69	2.01

The list of the systematic uncertainties for the measurement of charmonium mass differences is shown in Table 8.

Table 8: Systematic uncertainties in the measurement of charmonium mass differences (in MeV).

Systematic uncertainty	$M_{\chi_{c1}} - M_{\chi_{c0}}$	$M_{\chi_{c2}} - M_{\chi_{c0}}$	$M_{\eta_c(2S)} - M_{\eta_c(1S)}$
Including other states	0.03	0.11	0.01
Description of detector resolution	0.05	0.05	0.04
Description of signal resonances	0.01	0.01	0.19
Background model	0.02	0.10	0.24
2D fit functions	0.08	0.05	0.12
Momentum scale calibration	0.04	0.04	0.26
Total	0.11	0.17	0.42

8.4 Feynman diagrams for B_s^0 decays to ϕ mesons

In the SM the decay $B_s^0 \to \phi\phi$ proceeds via a gluonic penguin process, $b \to s\bar{s}s$, with four strange quarks in the final state. Its quark-level diagram is shown in Fig. 14.

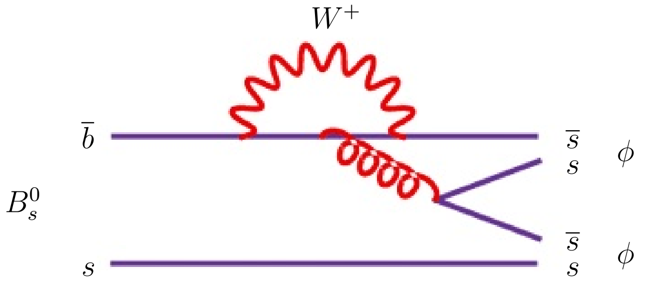

Figure 14: Diagram describing the $B_s^0 \to \phi\phi$ decay.

The three-body $B_s^0 \to \phi\phi\phi$ decay can be described by a penguin diagram shown in Fig. 15. This diagram is similar to the diagram describing the $B_s^0 \to \phi\phi$ decay mode, (Fig. 14) and involves creation of an additional $s\bar{s}$ quark pair. The transition thus leads to the final state with six strange quarks. Alternatively, this transition can proceed via intermediate resonances, e.g. $B_s^0 \to \eta_c(1S)(\to \phi\phi)\phi$, as shown in Fig. 16.

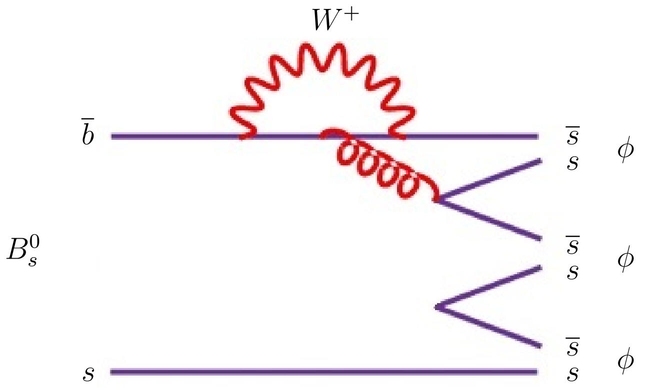

Figure 15: Diagram describing the three-body $B_s^0 \to \phi\phi\phi$ decay.

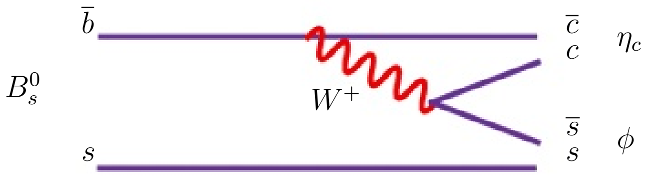

Figure 16: Diagram describing the $B_s^0 \to \eta_c\phi$ decay.

8.5 Symmetrized Dalitz plot to search for intermediate resonances in the $B_s^0 \to \phi\phi\phi$ decay

A symmetrized Dalitz plot is constructed following Ref. [59] for the B_s^0 signal region (Fig. 17, left) and sidebands ($4.925 - 5.325\,\text{GeV}$ and $5.415 - 5.815\,\text{GeV}$, Fig. 17, right), using the $X = \sqrt{3}(T_1 - T_2)/Q$ and $Y = 3T_3/Q - 1$ axes, where $T_{1,2,3}$ are kinetic energies of ϕ mesons in the rest frame of B_s^0 and Q is the energy released in the $B_s^0 \to \phi\phi\phi$ decay. The B_s^0 candidates are constrained to the known B_s^0 mass. No evidence for resonant contributions is observed within the available statistics.

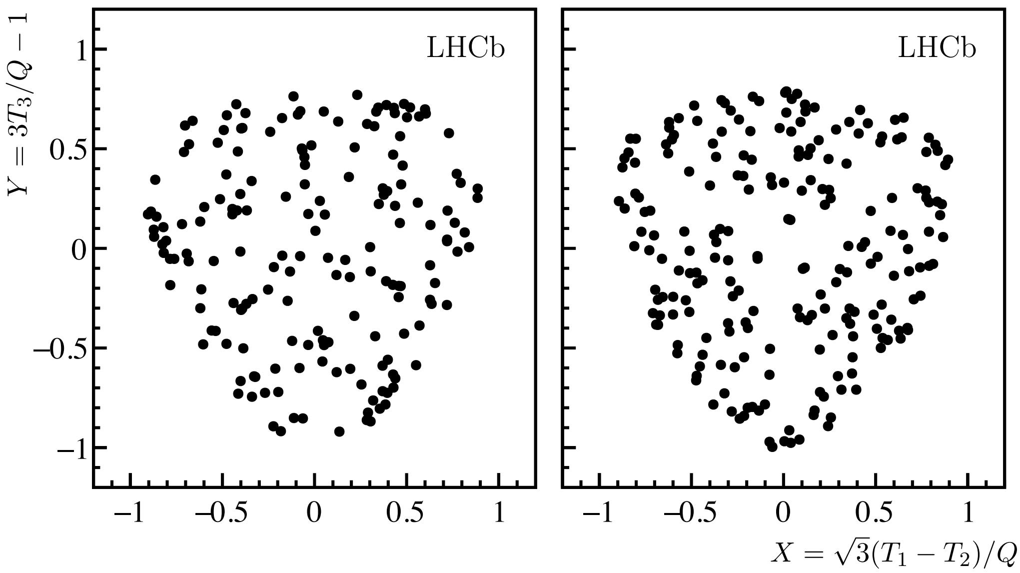

Figure 17: Symmetrized Dalitz plot [59] for (left) the B_s^0 signal and (right) the sideband regions. The B_s^0 candidates are constrained to the known B_s^0 mass.

8.6 Polarization of ϕ mesons in the $B_s^0 \to \phi\phi\phi$ decay

To quantify the fraction of transverse polarization, f_{T}, in the data, the probability density function (PDF) for f_{T} is shown in Fig. 18. The most probable value is $f_{\mathrm{T}} = 0.86$. Assuming a uniform prior in the physically allowed range, a Bayesian lower limit of $f_{\mathrm{T}} > 0.28$ at 95% CL is found.

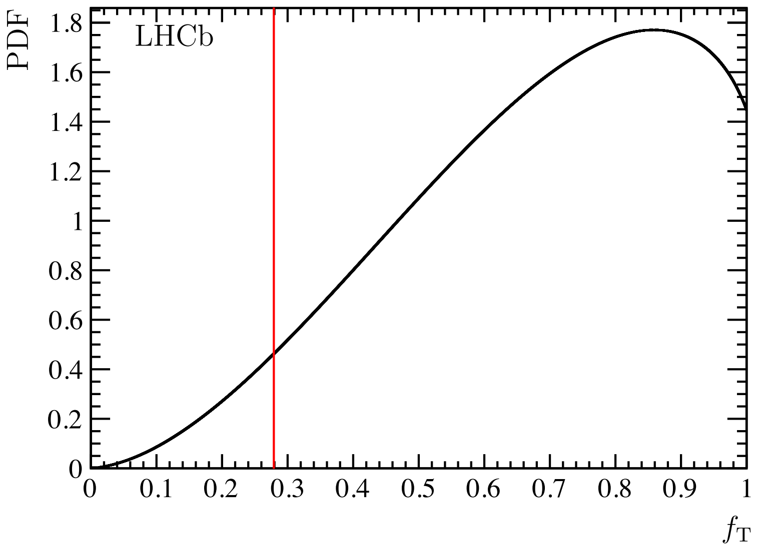

Figure 18: The PDF for the fraction of transverse ϕ meson polarization f_{T} for the $B_s^0 \to \phi\phi\phi$ candidates. The 95% Bayesian lower limit is shown by the red vertical line.